Equal Rights for Activators – Ytterbium to Terbium Cooperative Sensitization in Molecular Upconversion

Federico Pini, Richard Knighton, Lohona Soro, Loïc Charbonnière, Marta Natile, Niko Hildebrandt

Equal Rights for Activators - Ytterbium to Terbium Cooperative Sensitization in Molecular Upconversion

Federico Pini,[1,2,3] Richard C. Knighton,[4,5] Lohona K. Soro,[4] Loïc J. Charbonnière,[4] Marta M. Natile,* [1,2] and Niko Hildebrandt* [3,6,7]

[1] *Istituto di Chimica della Materia Condensata e Tecnologie per l'Energia (ICMATE), Consiglio Nazionale delle Ricerche (CNR), 35131 Padova PD, Italy.*
[2] *Dipartimento di Scienze Chimiche, Università di Padova, 35131 Padova PD, Italy.*
[3] *Laboratoire COBRA, Université de Rouen Normandie, CNRS, INSA Rouen, Normandie Université, France.*
[4] *Equipe de synthèse pour l'analyse (SynPA), Institut Pluridisciplaire Hubert Curien (IPHC), UMR 7178, CNRS/Université de Strasbourg, ECPM, 25 rue Becquerel, 67087 Strasbourg cedex, France.*
[5] *School of Chemistry, Main Building, Cardiff University, Cardiff, CF10 3AT, United Kingdom.*
[6] *Department of Chemistry, Seoul National University, Seoul 08826, South Korea.*
[7] *Department of Engineering Physics, McMaster University, Hamilton, ON L8S4L7, Canada.*

**Corresponding authors: martamaria.natile@unipd.it, hildebrandt@mcmaster.ca*

ABSTRACT

Molecular scaffolds are ideal to investigate upconversion (UC) at the highest spatial resolution and to create precisely controllable luminescent materials. Such control may be the key to overcome the limitations of brightness and reproducibility found in UC micro- and nanoparticles. Cooperative UC can significantly increase luminescence brightness and bulk studies showed that highest efficiencies can be obtained by sensitizer-to-activator ion ratios ≥ 2, i.e., via high probabilities of sensitizing the emitting lanthanide ion. Using nonanuclear molecular complexes, we demonstrate both experimentally and theoretically that interion distances are more relevant and that highest UC efficiencies are actually attained for sensitizer-to-activator ion ratios around 1. By modeling accretive and cooperative sensitization UC and energy migration and fitting to experimental data, we reveal that cooperative sensitization is predominant for the determination of UC luminescence intensities, whereas energy migration defines UC luminescence kinetics. The implementation of interion distances and different energy transfer mechanisms into advanced modeling of experimental UC data will be paramount for designing brighter and better UC materials.

KEYWORDS: *Upconverting complexes, Polynuclear complexes, Lanthanides, Terbium, Modeling*

Upconversion (UC) of near-infrared (NIR) to visible photons in solids,[1,2] submicron particles (UC phosphors)[3,4] and nanoparticles (UC nanoparticles),[5–7] and in solution (triplet-triplet annihilation)[8,9] has been studied for many years and applied to photovoltaics, photocatalysis, bioanalysis, or theranostics.[10–14] Despite the advances in material design and optimization, UC micro and nanoparticles have arguably reached the limits of brightness and reproducibility and new concepts are necessary for further improvements. Intramolecular UC within discrete molecular compounds is a recent approach that has the potential for advancing UC performance via precise molecular building blocks.[15–20] However, molecular UC is a very young research field that still requires a lot of fundamental investigations and understanding before experimental breakthroughs concerning brightness improvement can become reality. In the *status quo*, molecular complexes have shown to be extremely sensitive to deactivation processes, such as vibrational losses to the ligand or solvent molecule overtones, which result in significantly lower UC efficiencies compared to UC phosphors or UC nanoparticles.[21–23] Different concepts, such as sensitization of the Er activator via an energy transfer UC (ETU) mechanism from organic dye antennas,[24–26] cooperative luminescence from numerous Yb ions,[27] or cooperative sensitization UC (CSU) via two sensitizers to brighter Tb or Ru activators,[20,28,29] have been developed with the aim to increase molecular UC luminescence (UCL) signals. Although experimental advances have resulted in more efficient molecular UC complexes, synthetic approaches alone will not be sufficient to accomplish brightness levels that can compete with UC nanoparticles. In nano, micro, and bulk crystalline materials, theoretical understanding and modeling of the different sensitization and deactivation processes between sensitizers, activators, and their environment have been studied in detail for ETU[30–32] and CSU[33,34] processes, and that knowledge has advanced UC nanoparticles to widely applied luminescent materials. However, the exact same principles that were established for those crystalline materials are not applicable to molecular UC complexes and thus, new models are paramount to better understand and improve molecular UC. This is especially true for the relatively young research field of molecular UC, for which UCL quantum yields accomplished so far span five orders of magnitude from 10^{-9} to 10^{-4}

(**Supporting Figure S1**). A recent study showed that co-crystallization of molecular UC complexes can lead to UC quantum yields that are even close to those of UCNPs.[35] To accelerate the advancement of UC molecules to actual applications and not rely on decades of optimization, as previously done for UCNPs, the implementation of advanced modeling is clearly a key solution.

Recently, we reported the synthesis and characterization of a combinatorial library of hetero-nonanuclear lanthanide complexes ($[Ln_9(acac)_{16}(OH)_{10}]OH$), including a detailed experimental investigation of their UC properties in solution.[28] The complexes' stoichiometries covered the range of all possible combinations of trivalent Yb ions as sensitizers (energy donors), Tb ions as activators (energy acceptors), and Y ions as spectroscopically silent surrogates, such that the final stoichiometry was $Tb_xYb_yY_z$ (with x, y, and z integer values and $x+y+z = 9$). Whereas some of the studied UC properties met the expectations based on the current state-of-the-art (e.g., excitation power dependence, UCL lifetime, effect of deuterium substitution in the ligands), the stoichiometry for the brightest complex was unexpected. Because CSU is a sensitized process (from at least two Yb sensitizers to one Tb activator), it would have been expected that higher ratios of Yb-per-Tb result in higher UC efficiency.[2,36] However, the most efficient UCL was found for Tb/Yb (i.e., x/y) ratios close to unity (4/5 or 5/4),[28] a phenomenon also observed for other molecular UCL devices.[16,37]

Considering a statistical distribution, the *nominal stoichiometry* (of the used lanthanide ion concentrations in the fabrication of the complexes) does not equal the *actual stoichiometry* (within the actually formed complexes), which explained why in our experimental study even for nominal Tb_8Yb_1 complexes significant UCL was observed.[28] Considering a statistical distribution of the Ln atoms in the complex, the actually formed complexes contained more than 26% of species with two or more Yb ions because the probability of complexes with an actual stoichiometry Tb_iYb_j formed from a nominal Tb_xYb_y composition is:

$$P_{i,j} = \frac{n!}{i!\,j!}\left(\frac{x}{n}\right)^{i}\left(\frac{y}{n}\right)^{j} \quad (1)$$

Here, *n* stands for the number of Ln ions in the complex, with *n* = 9 in our case of nonanuclear complexes. Whereas this probability distribution also shows that the maximum fraction of CSU complexes is formed for *x*/*y* ratios between circa 3/6 and 6/3 (**Figure 1**), it does not explain why the most efficient UCL was found for *x*/*y* ratios of 5/4 and 4/5.

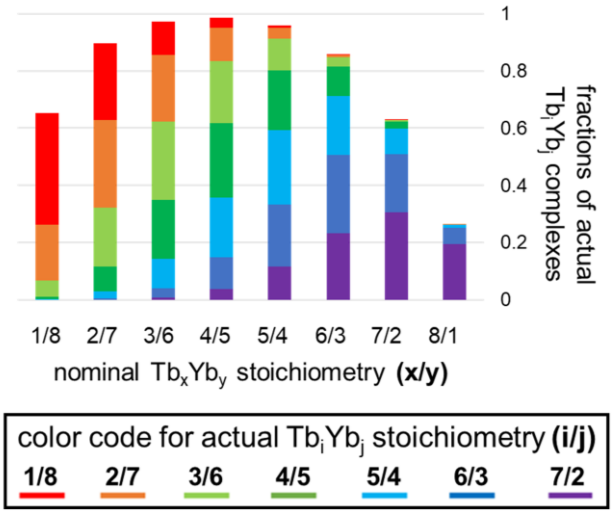

Figure 1. Fractions of actually formed Tb_iYb_j nonanuclear complexes as a function of nominal Tb_xYb_y mixtures (*x*/*y* presents the Tb-to-Yb concentration ratio).

To understand the difference between the expected and experimentally obtained UCL, the complete distribution of Tb and Yb ions and their interionic distances, which define the strengths of energy transfer interactions between the ions, must be accounted for, and the overall CSU must be calculated from the entire set of actual complex conformations. As mentioned above, a nominal stoichiometry (input concentrations for synthesis of the complexes) of Tb_xYb_y will produce a close-to statistical distribution of possible complexes with real or actual stoichiometry of Tb_iYb_j. Each of these actual complexes will then result in a family of configurations (isomers), in which the Tb and Yb ions can randomly occupy any of the nine different possible sites of the complex's square bipyramidal skeleton. Disregarding the symmetry elements of the nonanuclear complex this leads to 9 Tb_1Yb_8, 36 Tb_2Yb_7, 84 Tb_3Yb_6, 126 Tb_4Yb_5, 126 Tb_5Yb_4, 84 Tb_6Yb_3, and 36 Tb_7Yb_2 possible CSU isomers (**Supporting Figure S2**). From X-ray crystallography of the Tb_4Yb_5 isomer, the relative possible positions of each lanthanide and thus, their interion distances are known. Single crystals suitable for analysis by X-ray crystallography (**Supporting Information**) were obtained for

the $[Tb_xYb_y(acac)_{16}(OH)_{10}]OH$ complex (x = 4.5, y = 4.5) from a solution of concentrated MeOH cooled to -18°C and the data were collected at 100±2 K. The compound crystallizes in the *P*4/*n* space group and is isostructural and isomorphous with previously reported Ln_9 clusters.[28] The structure (**Figure 2A**) displays a nonanuclear core, consisting of two square-based pyramids which share the central Ln vertex, such that the overall structure is that of an hour-glass arrangement, with the top and bottom half rotated by *ca*. 45°. The Ln center is octacoordinated, ligated by eight μ_3-OH ligands. The remaining eight atoms are eight coordinated, connected by two μ_3-OH, one μ_4-O/OH bridge, and five oxygens from one bidentate and two bridging acetylacetonate ligands. The cluster displays local four-fold symmetry in the solid-state, meaning only one top and bottom vertex are crystallographically unique, exhibiting perfect squares on the top and bottom faces (90.0000±0.0013° and 90.00000±0.00018°). The pertinent interatomic distances (**Figure 2A** and **Supporting Figure S4**) were determined to be 3.5931±0.0003 Å (Ln1–Ln1 and Ln3–Ln3) for the square edges and 5.0317±0.0004 Å (Ln1–Ln1') or 5.0814±0.0004 Å (Ln3–Ln3') for the base diagonals. The largest intra-cluster ion distance was 7.1385±0.0003 Å (Ln1–Ln3'). Comparison of the single-crystal X-ray diffraction metrics of the heterometallic $Tb_{4.5}Yb_{4.5}$ mixture in comparison to a previously reported Tb_9 homologue revealed only a small covariance between the two (**Supporting Table S1**).[38] Overall, the intermetallic distances were elongated in the homometallic cluster, due to the larger radius of Tb^{III} *vs*. Yb^{III}, showing deviations typically below 1% between the two structures. This demonstrates that changes in interion distance are negligible when considering the Tb-Tb, Tb-Yb, and Yb-Yb distances in co-doped clusters. Once exactly assessed the positions of the lanthanides in the clusters, what will change through the configurations is the ion-to-ion distance distribution, which determines the figure of merit for CSU.

Using a purposely developed Python code (cf. **Supporting Information**), we simulated all the $N_{i,j}$ isomer configurations for each Tb_iYb_j complex to calculate the final distribution of Yb-to-Yb, Tb-to-Tb, and Yb-to-Tb average distances (**Figure 2**).

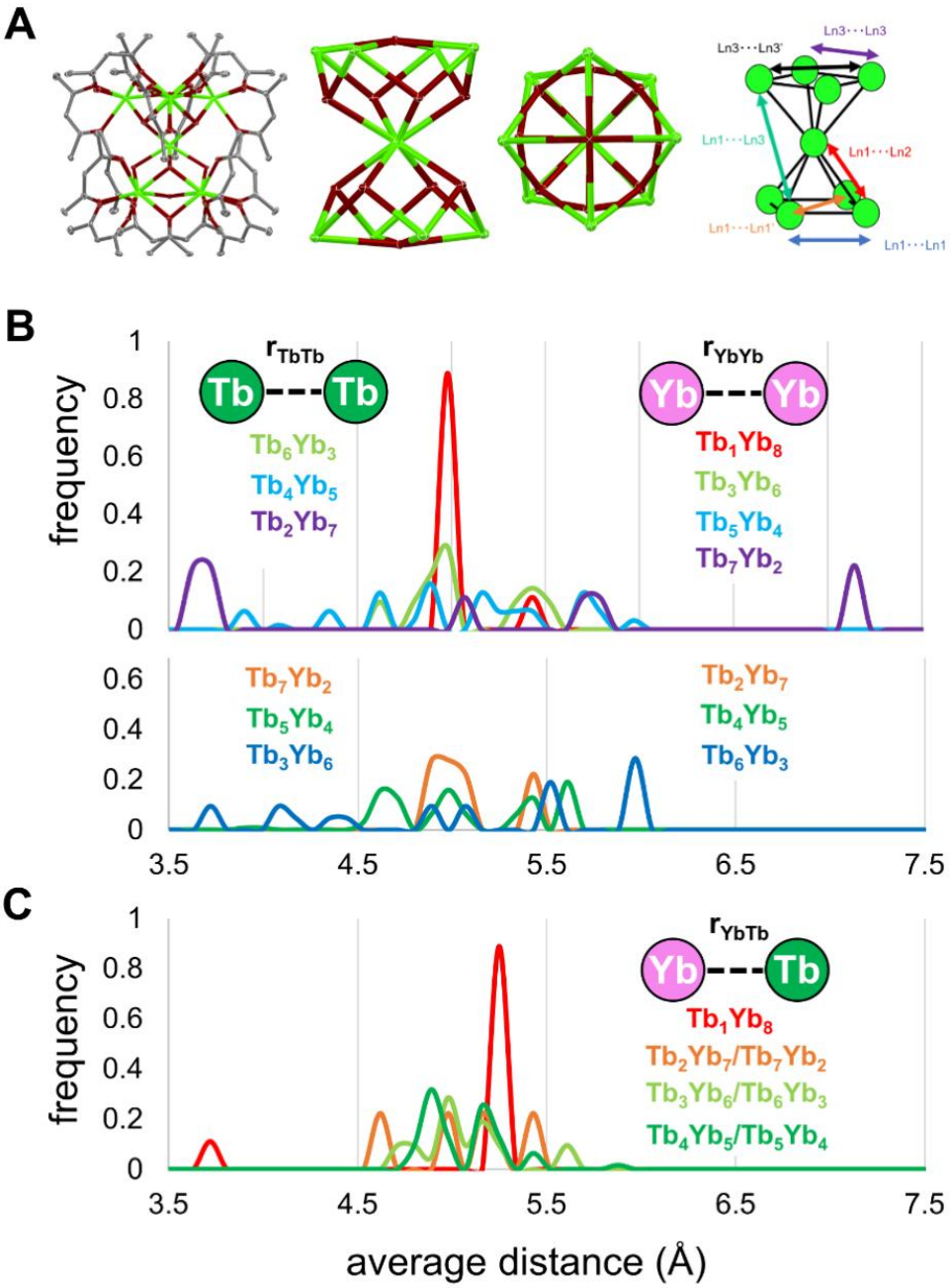

Figure 2. (**A**) Single-crystal X-ray structure of a $[Tb_xYb_y(acac)(OH)_{10}]OH$ complex (x = 4.5, y = 4.5), from left to right: full structure; nonanuclear $Ln_9(OH)_8$ core; top-down view of $Ln_9(OH)_8$ core (H-atoms and solvent molecules omitted for clarity, ellipsoids plotted at the 50% probability level); schematic depiction of the nonanuclear core showing only the lanthanide nuclei and including atom numbering for specific interion distances (CCDC no. 2333808). Frequency distribution of the average Yb-to-Yb , Tb-to-Tb (**B**), and Yb-to-Tb (**C**) distances (r) calculated for all isomer configurations of a given Tb_iYb_j complex. Tb_8Yb_1, Tb_9Yb_0, and Tb_0Yb_9 are not included because at least 2 Yb ions and 1 Tb ion are necessary for CSU.

The Yb-to-Yb average distance distribution becomes narrower with increasing amounts of Yb. For example, for Tb_1Yb_8 (red curve in **Figure 2B**) all average Yb-Yb distances are within a 5 to 5.5 Å range, for Tb_4Yb_5 (dark green curve in **Figure 2B**) the distribution broadens to a range between 4 and 6 Å, and for Tb_7Yb_2 (purple curve in **Figure 2B**) the Yb-Yb distances are broadly

distributed between circa 3.5 and 7.3 Å. For Tb-to-Tb distances, the distributions are a mirror of the Yb/Yb configurations with an inverted trend of narrowing with increasing amounts of Tb. For Tb-to-Yb distances (**Figure 2C**), the distributions are narrower because they are the same for Tb_iYb_j and Tb_jYb_i. Notably, the distribution becomes more compact for the complexes with Tb-to-Yb ratios close to one. The only complex which does not have a symmetrical analog is Tb_1Yb_8 (because Tb_8Yb_1 cannot produce CSU). For this complex, the distance distribution provides only two possible distances, for which 5.25 Å corresponds to the Tb ion in one of the two bases of the bipyramid and 3.72 Å corresponds to the Tb ion on the vertex of the two pyramids. This assignment is also confirmed by the probability of the two distances, with the shorter one being eight times less probable than the longer one.

To calculate the actual UCL contributions, the statistical distribution of actual complexes and the interion distance distributions within all possible complex configurations need to be combined with CSU probability laws. Lanthanide energy transfer probabilities have been investigated in bulk systems (*e.g.*, solid state laser materials and solutions), microsystems (*e.g.*, powders and microparticles), and nanosystems (*e.g.*, UC and other NPs) for many years.[39–42] Despite the development of several sophisticated models for understanding energy transfer processes,[43–45] several of their bulk-system approximations (*e.g.*, large number of ions and isotropy of the system) are not applicable to molecular systems. Although the fundamental ET interactions, *i.e.*, electrostatic multipolar interaction (Förster-like)[46,47] and exchange interaction through wavefunction overlap (Dexter-like),[48,49] apply to any system from the molecular to the bulk scale, the distinction between these two mechanisms is difficult from experimental data of complex systems, in particular, for cooperative processes. For this reason, we focused our analysis on multipolar interaction cooperative ET probabilities.

Kushida and Auzel proposed two concurring mechanisms of CSU,[1,47] which can be defined as accretive and cooperative, in analogy to downconversion (i.e., quantum cutting). Both mechanisms require polarization induced by a virtual state of opposite parity. In the accretive one

(P_{Ac}, **Equation 2**) the virtual state is localized on one of the Yb ions, thus the excitation must firstly pass from another Yb to the virtual state and then, when this state is charged, to the Tb acceptor. For this reason, the accretive mechanism depends on both Yb-Yb and Yb-Tb distances. On the other hand, the cooperative mechanism probability (P_{Co}, **Equation 3**) depends only on Yb-Tb distances because the virtual state is located on the acceptor (Tb), which gets charged by ET from two Yb, disregarding the mutual position of the two sensitizers, and then transfer the energy to the Tb ion.[50] The probability law was firstly derived by Kushida for a trimeric system composed of two sensitizers (Yb) and one activator (Tb). Here we adapted the approach to multimeric systems,[47] similar to what was first proposed by Inokuti and Hirayama and later adapted algorithmically by Vergeer *et al.* for quantum cutting in nanomaterials.[45,50] As outlined in our previous work,[28] the increase of the nominal fraction of Yb in the complexes led to a decrease in the UCL lifetime (**Figure S3A**), which suggests the presence of energy migration (EM) via Yb ions, similarly to what has been observed in nanomaterials.[51,52] Thus, we also included an EM probability (P_{EM}, **Equation 4**) in our theoretical model. EM describes the transfer of energy from an excited-state Yb ion to a ground-state Yb ion in close proximity. This energy migration can lead to very beneficial effects in nano- and micromaterials because it allows excitons to migrate over long distances to reach the emitting activator ions. On the other hand, it can also have detrimental effects because it can trap the exciton in quenchable (dark) states and facilitate migration to the particle surface, which is heavily exposed to the UCL-quenching environment.[53] For the small dimensions of molecular UC complexes in diluted solutions, migration over long distances is not possible. Therefore, energy migration can only result in detrimental effects that facilitate the loss of excitons through deactivation of Yb ions. EM via Tb ions is in principle also possible and was included in our initial model. However, the experimental data could be adequately fit without the Tb-Tb interaction term and thus, to avoid an over-parametrization of the problem, we decided to omit Tb-Tb EM. A probable explanation of the minor influence of Tb-Tb EM compared to Yb-Yb EM is the larger Tb energy gap, which results in a significantly lower quenching probability.

$$P_{\mathrm{Ac}} = A_{\mathrm{AC}} \sum_{a}^{N_{\mathrm{Yb}}} \sum_{b\neq a}^{N_{\mathrm{Yb}}} \sum_{c}^{N_{\mathrm{Tb}}} \left(\frac{1}{\left(r_{\mathrm{Yb_aYb_b}}\, r_{\mathrm{Yb_aTb_c}}\right)^{2\mathrm{p}}} + \frac{1}{\left(r_{\mathrm{Yb_aYb_b}}\, r_{\mathrm{Yb_bTb_c}}\right)^{2\mathrm{p}}} \right) \quad (2)$$

$$P_{\mathrm{Co}} = A_{\mathrm{Co}} \sum_{\mathrm{a}}^{\mathrm{N_{Yb}}} \sum_{c}^{\mathrm{N_{Tb}}} \frac{1}{\left(r_{\mathrm{Yb_aTb_c}}\right)^{4\mathrm{p}}} \quad (3)$$

$$P_{\mathrm{EM}} = A_{\mathrm{EM}} \sum_{\mathrm{a}}^{\mathrm{N_{Yb}}} \sum_{b\neq a}^{\mathrm{N_{Yb}}} \frac{1}{\left(r_{\mathrm{Yb_aYb_b}}\right)^{2\mathrm{p}}} \quad (4)$$

The accretive probability (**Equation 2**) contains a triple summation over the indices of Yb (*a* and *b*, which must be different) and Tb ions (*c*), which describe the positions in which the ions are placed inside the complex structure. The cooperative probability (**Equation 3**) depends solely on Yb-to-Tb distances, whereas the EM probability (**Equation 4**) depends only on Yb-to-Yb distances and would present a negative contribution to UCL. The distances (*r*) are those between the different ions in the different positions (*a*, *b*, and *c*) within the complex structures. The parameter *p* determines the type of interaction between ions, which can be 3, 4, etc. for dipole-dipole, dipole-quadrupole, etc.. Trials with different values of *p* led to minor differences in the resulting probabilities and thus, we used the dipole-dipole interaction with $p = 3$. The parameters A_{Ac}, A_{Co}, and A_{EM} present the probability amplitudes, which have units Å^{12} for cooperative and accretive mechanisms and Å^{6} for energy migration, in order to obtain dimensionless probabilities.

Equations 2, **3** and **4** were used to calculate the different expected probabilities for each configuration within each actual stoichiometry. The average of those distinct probabilities provided the overall probability of accretive CSU, cooperative CSU, and EM for each actual nonanuclear Tb_iYb_j complex (**Figure 3A**). As expected, the EM probability (grey line in **Figure 3A**) increased with increasing fractions of Yb and showed a difference of ~100% between Tb_7Yb_2 and Tb_1Yb_8. Cooperative CSU (orange line in **Figure 3A**) as a function of *i/j* stoichiometry appeared as a symmetric bell shape, mimicking the Yb-to-Tb distance distribution, and showing maximum probabilities for Tb_4Yb_5 and Tb_5Yb_4 complexes. These results suggest that the narrower the average interion distance distribution (cf. **Figure 2**) the higher the CSU probability. Accretive CSU (blue line in **Figure 3A**) contains both Yb-to-Yb and Tb-to-Yb contributions, which resulted in a

probability function with unsymmetric bell shape that was shifted to Yb-richer complexes with a maximum for Tb_3Yb_6. Importantly, the CSU probabilities for these actual complexes differ from the expectation that more Yb sensitizers would lead to stronger CSU. This result is strongly connected to the interion distances within the complexes and is therefore dependent on the complex composition and not only on the fraction of sensitizers and activators.

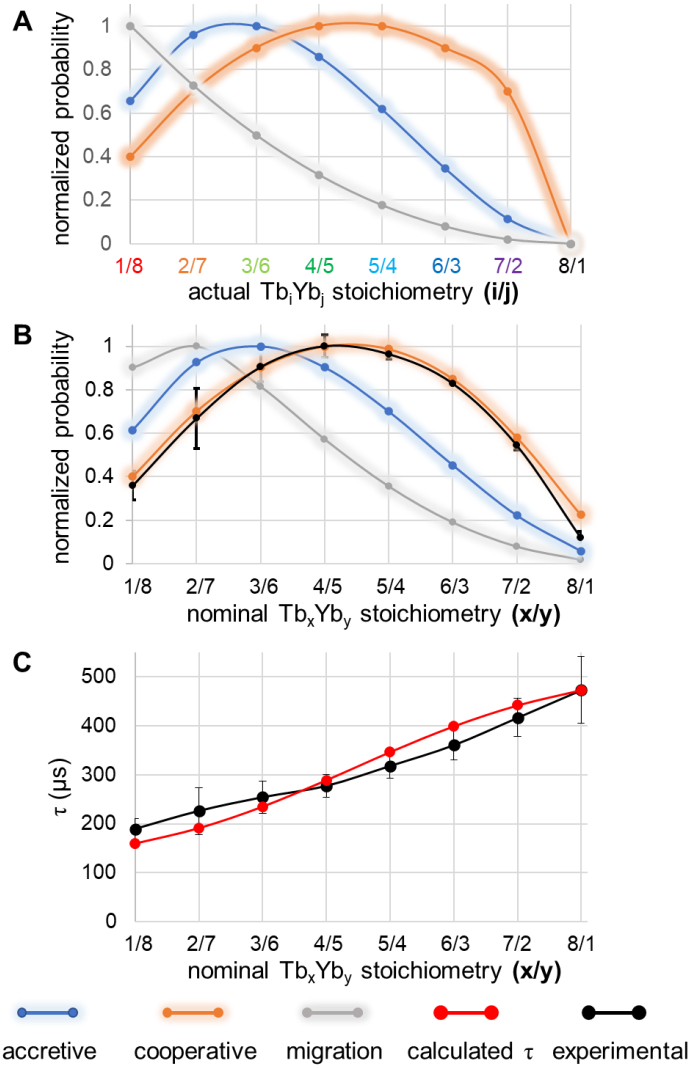

Figure 3. Normalized probabilities of accretive CSU (blue), cooperative CSU (orange), and EM (gray) for each actual Tb_iYb_j complex (**A**) and each nominal Tb_xYb_y complex (**B**). Same colors are showed for the respective probabilities in B, while black curve in B shows the experimental CSU obtained from UCL decay curves (cf. **Supporting Figure S3**). (**C**) Normalized average UCL lifetimes for each nominal Tb_xYb_y complex: calculated (red line) and experimental (black curve). The black curve was derived from bi-exponential fitting of the UCL decay curves (cf. **Supporting Figure S3**). The error bars in B and C present standard deviations from measuring three independently prepared samples.

To model the actual experimental results, the probabilities of each phenomenon for the nominal complex stoichiometries Tb_xYb_y are required. These were obtained by multiplying the

probability of accretive CSU, cooperative CSU, and EM (**Figure 3A**) by the probability of having a certain actual complex (Tb_iYb_j) given a nominal stoichiometry (cf. **Equation 1** and **Figure 1**). The results (**Figure 3B**) show that maximum probabilities were obtained with Tb_2Yb_7 (i.e., x/y = 2/7) for EM, with Tb_4Yb_5 (i.e., x/y = 4/5) for cooperative CSU, and with Tb_3Yb_6 (i.e., x/y = 3/6) for accretive CSU. Notably, the cooperative mechanism for CSU (orange curve in **Figure 3B**) mimics almost perfectly the experimental CSU data (black curve in **Figure 3B**), which represent UCL intensities calculated from UCL kinetics with long (60 µs) excitation pulses. This result shows that the accretive mechanism, as pointed out in quantum cutting studies,[50] and EM are not required to explain the experimental CSU intensity data for the nonanuclear molecular UC complexes. Nevertheless, both mechanisms may be important to describe the UCL intensities of other UC complexes. In that case, the sum of all three mechanisms can be fit to the experimental data to calculate the contribution of each to the overall UCL intensity.

Interestingly, our model can also predict ETU probabilities for molecular UC complexes. Again, nonanuclear complexes with equal amounts of sensitizers and activators were identified as the best system (i.e., x/y and i/j ratios of 4/5 and 5/4 – cf. **Supporting Equation S1 and Figure S5**), which is in strong contrast to the optimum sensitizer-activator ratios in UC phosphors or nanoparticles that are usually around 9 (18% Yb and 2% Er).[54,55] Unfortunately, sufficiently bright UCL could not be accomplished with ETU in our nonanuclear complexes because the common ETU activator ions, such as Er or Tm, are much less bright than Tb CSU activators. Nevertheless, the theoretical prediction of highest ETU probability in nonanuclear complexes via sensitizer-activator ratios around unity shows that unprecedented and possibly brighter materials may become accessible via molecular UC. If ETU complexes including more than three ions can be developed in the future, it would be highly interesting to apply our model and verify this theoretical assumption.

Although EM was not required to explain the experimental CSU intensities, it can be very useful to model the CSU lifetimes, since these showed a clear dependence on the Yb content (black line in **Figure 3C**). The expression of the calculated average CSU lifetime for each nominal (x/y)

composition ($\tau_{x,y}$, **Equation 5**) can be written as the weighted average of the lifetimes of the actual (i/j) complexes ($\tau_{i,j}$), where the weighting factor ($\alpha_{i,j}$) describes the probability ($P_{i,j}$) to obtain an actual composition given a nominal one. The complex stoichiometry-dependent CSU lifetime is determined via the population and depopulation of Yb ion energy levels (cf. **Supporting Information**). Therefore, the CSU lifetime of each actual stoichiometry can be expressed as the sum of all processes leading to the deactivation of Yb ions for each complex, i.e., the deactivation of the isolated ion (k_0) and *EM*.

$$\tau_{x,y} = \sum_{(i,j)} \alpha_{i,j}\tau_{i,j} = \frac{\sum_{(i,j)} P_{i,j}\tau_{i,j}}{\sum_{(i,j)} P_{i,j}} \quad (5)$$

$$\tau_{i,j} = \frac{1}{k_0 + EM} = \frac{\tau_0}{\left(1 + P_{EM}^{i/j}\right)} \quad (6)$$

Using **Equations 5** and **6** we were able to compare the experimental average lifetimes for each nominal stoichiometry *x*/*y* (**Figure S2)** with the calculated ones. When fitting the experimental UCL lifetimes (black curve in **Figure 3C**) with **Equation 5**, $P_{i,j}$ was fixed and determined from statistical considerations (**Equation 1**). $P_{EM}^{i/j}$ (the energy migration probability for a given actual composition, **Equation 4**) was determined by the distance distribution and by the amplitude parameter A_{EM}. Thus, the only fit parameters to obtain the calculated lifetimes were τ_0 and A_{EM}. The optimal values for these parameters were τ_0 = 475 µs and A_{EM} = 2630 Å^6, which reproduced the experimental average lifetime with very good accuracy (red curve **Figure 3C**) and confirmed the initial hypothesis of an important contribution of EM to the CSU lifetimes. The finding that EM did not play a role for the determination of CSU intensities but significantly contributed to the CSU lifetimes may seem counterintuitive. However, UCL is dependent on many energy levels, energetic transitions, and interactions between different ions, which can result in a dominant contribution of the cooperative mechanism for CSU intensities, whereas the decay kinetics from the final excited state may still be strongly influenced by EM. Another explanation would be an equilibrium between the accretive mechanism (positive contribution for CSU intensities) and EM (negative contribution for CSU intensities), where one contribution compensates the other (because of their similar

dependence on nominal stoichiometry – **Figure 3B**), such that only the cooperative mechanism determines the overall CSU intensity.

Including the luminescence lifetime of the Yb sensitizers or the risetime of the Tb UCL in the analysis and modeling could in principle provide an even better understanding of the entire molecular UC process. Yb emission can be observed upon both ligand and Tb excitation via downshifting.[28] For our complexes, Yb downshifting luminescence lifetimes were 15 µs for Yb_9, 17 µs for Tb_1Yb_8, 18 µs for Tb_3Yb_6, and 20 µs for Tb_4Yb_5, and Tb UCL lifetimes were 189 µs for Tb_1Yb_8, 254 µs for Tb_3Yb_6, and 277 µs for Tb_4Yb_5.[28] Due to the significantly stronger change in the UCL lifetimes, our model focused on UCL only. With the same aim of using as few parameters as possible for a simple but still accurate analytical model, we also omitted the risetime parts of the Tb UCL. However, we also developed a semi-analytical model that could fit the complete (rise and decay) UCL kinetics and also validated our simpler and more intuitive analytical approach (**Supporting Information**).

In conclusion, we theoretically confirmed the experimental findings that similar amounts (ratio close to one) of sensitizers and activators result in the highest UC efficiencies in molecular CSU complexes. This result is highly important as it has been commonly assumed that large ratios of sensitizers per activators lead to high UCL efficiencies because more sensitizers should provide a higher probability of sensitizing the emitting activator ion. Because brightness is also influenced by the absorption cross section and the quenching of the sensitizers (both increase with the number of sensitizers), the sensitizer-to-activator ratio cannot be too high either. However, ratios ≥2 are considered to be beneficial for UC brightness. Whereas this assumption may be true for systems with equal distances between all ions and in large upconversion ensembles (i.e., nano or microparticles), for which energy migration over long distances is necessary to efficiently reach the final activator ion, it is not a general fact for upconversion. Using nonanuclear complexes, in which Yb sensitizers and Tb activators in Tb/Yb concentration ratios between 1/8 and 8/1 were allowed to take any possible position within the complexes, we demonstrated experimentally that ratios close

to unity (i.e., 5/4 and 4/5) yielded the brightest UCL. This finding was confirmed by a theoretical model that calculated the contributions of accretive CSU, cooperative CSU, and EM based on all possible interion distances in the nonanuclear complexes. The model provided excellent concordance with the experimental data when only the cooperative mechanism was taken into account for CSU. Our results showed that interion distances (and not sensitizer/activator ratios) are the most important parameter for the determination of UC efficiencies and that accretive CSU and EM played minor roles for UCL intensities in the nonanuclear complexes. Interestingly, the model also predicted highest UCL efficiencies for ETU-based nonanuclear complexes (e.g., Yb sensitizers and Er activators). However, due to their very low brightness, such ETU complexes could unfortunately not be investigated experimentally. Despite the predominance of cooperative CSU in UCL intensity, EM could be used to model the UCL decays with very good fit between the model and the experimental data. Our approach of combined theoretical modeling and experimental analysis of the UCL decays provided a better understanding of the mechanisms that drive UCL intensity and decay kinetics in molecular upconversion and showed that interion distance is extremely important when studying upconversion on a molecular scale. Considering that our model can be applied for any upconversion system for which interion distances are known, our results are also important for reconsidering the mechanisms of upconversion in general and to stimulate the appreciation and careful analysis of interion distances also for designing more efficient upconversion nanoparticles.

ACKNOWLEDGMENTS

This work was financed by Université Franco-Italienne (UFI, PhD fellowship of Federico Pini), the French Agence Nationale de la Recherche (project LAPIN – ANR-20-CE09-0021-04, project LUCAS n° ANR-19-CE29-0014-01), the Brain Pool program funded by the Ministry of Science and ICT through the National Research Foundation of Korea (2021H1D3A2A02049589), Seoul National University, Université Rouen Normandie, INSA Rouen Normandie, Centre National de la Recherche Scientifique, the European Regional Development Fund, Labex SynOrg (ANR-11-LABX-0029), Carnot Institute I2C, XL-Chem graduate school (ANR-18-EURE-0020 XL CHEM), Région Normandie, the program of scientific cooperation CNR/CAS 2019-2022, Istituto di Chimica

della Materia Condensata e Tecnologie per l'Energia, Consiglio Nazionale delle Ricerche, Dipartimento di Scienze Chimiche, Università di Padova, and the Canada Excellence Research Chairs Program (CERC in Nano-Optical Biosensing and Molecular Diagnostics, CERC-2022-00072).

REFERENCES

(1) Auzel, F. Upconversion Processes in Coupled Ion Systems. *J. Lumines.* **1990**, *45* (1–6), 341–345. https://doi.org/10.1016/0022-2313(90)90189-I.
(2) Auzel, F. Upconversion and Anti-Stokes Processes with f and d Ions in Solids. *Chem. Rev.* **2004**, *104* (1), 139–174. https://doi.org/10.1021/cr020357g.
(3) Wright, W. H.; Mufti, N. A.; Tagg, N. T.; Webb, R. R.; Schneider, L. V. High-Sensitivity Immunoassay Using a Novel Upconverting Phosphor Reporter. In *Ultrasensitive Biochemical Diagnostics II*; Proceedings of SPIE 2985; SPIE, 1997; Vol. 2985, pp 248–255. https://doi.org/10.1117/12.274357.
(4) Soukka, T.; Kuningas, K.; Rantanen, T.; Haaslahti, V.; Lövgren, T. Photochemical Characterization of Up-Converting Inorganic Lanthanide Phosphors as Potential Labels. *J. Fluoresc.* **2005**, *15* (4), 513–528. https://doi.org/10.1007/s10895-005-2825-7.
(5) Resch-Genger, U.; Gorris, H. H. Perspectives and Challenges of Photon-Upconversion Nanoparticles - Part I: Routes to Brighter Particles and Quantitative Spectroscopic Studies. *Anal. Bioanal. Chem.* **2017**, *409* (25), 5855–5874. https://doi.org/10.1007/s00216-017-0499-z.
(6) Gnach, A.; Lipinski, T.; Bednarkiewicz, A.; Rybka, J.; Capobianco, J. A. Upconverting Nanoparticles: Assessing the Toxicity. *Chem. Soc. Rev.* **2015**, *44* (6), 1561–1584. https://doi.org/10.1039/C4CS00177J.
(7) Haase, M.; Schäfer, H. Upconverting Nanoparticles. *Angew. Chem. Int. Ed.* **2011**, *50* (26), 5808–5829. https://doi.org/10.1002/anie.201005159.
(8) Parker, C. A.; Hatchard, C. G.; Bowen, E. J. Delayed Fluorescence from Solutions of Anthracene and Phenanthrene. *Proc. R. Soc. London, Ser. A* **1997**, *269* (1339), 574–584. https://doi.org/10.1098/rspa.1962.0197.
(9) Yanai, N.; Kimizuka, N. New Triplet Sensitization Routes for Photon Upconversion: Thermally Activated Delayed Fluorescence Molecules, Inorganic Nanocrystals, and Singlet-to-Triplet Absorption. *Acc. Chem. Res.* **2017**, *50* (10), 2487–2495. https://doi.org/10.1021/acs.accounts.7b00235.
(10) Kuningas, K.; Rantanen, T.; Ukonaho, T.; Lövgren, T.; Soukka, T. Homogeneous Assay Technology Based on Upconverting Phosphors. *Anal. Chem.* **2005**, *77* (22), 7348–7355. https://doi.org/10.1021/ac0510944.
(11) Sun, G.; Xie, Y.; Sun, L.; Zhang, H. Lanthanide Upconversion and Downshifting Luminescence for Biomolecules Detection. *Nanoscale Horiz.* **2021**, *6* (10), 766–780. https://doi.org/10.1039/D1NH00299F.
(12) Richards, B. S.; Hudry, D.; Busko, D.; Turshatov, A.; Howard, I. A. Photon Upconversion for Photovoltaics and Photocatalysis: A Critical Review. *Chem. Rev.* **2021**, *121* (15), 9165–9195. https://doi.org/10.1021/acs.chemrev.1c00034.
(13) Wang, Y.; Song, S.; Zhang, S.; Zhang, H. Stimuli-Responsive Nanotheranostics Based on Lanthanide-Doped Upconversion Nanoparticles for Cancer Imaging and Therapy: Current Advances and Future Challenges. *Nano Today* **2019**, *25*, 38–67. https://doi.org/10.1016/j.nantod.2019.02.007.
(14) Tessitore, G.; Mandl, G. A.; Brik, M. G.; Park, W.; Capobianco, J. A. Recent Insights into Upconverting Nanoparticles: Spectroscopy, Modeling, and Routes to Improved Luminescence. *Nanoscale* **2019**, *11* (25), 12015–12029. https://doi.org/10.1039/C9NR02291K.
(15) Aboshyan-Sorgho, L.; Besnard, C.; Pattison, P.; Kittilstved, K. R.; Aebischer, A.; Bünzli, J.-C. G.; Hauser, A.; Piguet, C. Near-Infrared→Visible Light Upconversion in a Molecular Trinuclear d–f–d Complex. *Angew. Chem. Int. Ed.* **2011**, *50* (18), 4108–4112. https://doi.org/10.1002/anie.201100095.
(16) Nonat, A. M.; Charbonnière, L. J. Upconversion of Light with Molecular and Supramolecular Lanthanide Complexes. *Coord. Chem. Rev.* **2020**, *409*, 213192. https://doi.org/10.1016/j.ccr.2020.213192.

(17) Bolvin, H.; Fürstenberg, A.; Golesorkhi, B.; Nozary, H.; Taarit, I.; Piguet, C. Metal-Based Linear Light Upconversion Implemented in Molecular Complexes: Challenges and Perspectives. *Acc. Chem. Res.* **2022**, *55* (3), 442–456. https://doi.org/10.1021/acs.accounts.1c00685.
(18) Golesorkhi, B.; Fürstenberg, A.; Nozary, H.; Piguet, C. Deciphering and Quantifying Linear Light Upconversion in Molecular Erbium Complexes. *Chem. Sci.* **2019**, *10* (28), 6876–6885. https://doi.org/10.1039/C9SC02068C.
(19) Golesorkhi, B.; Nozary, H.; Fürstenberg, A.; Piguet, C. Erbium Complexes as Pioneers for Implementing Linear Light-Upconversion in Molecules. *Mater. Horiz.* **2020**, *7* (5), 1279–1296. https://doi.org/10.1039/C9MH01899A.
(20) Knighton, R. C.; Soro, L. K.; Thor, W.; Strub, J.-M.; Cianférani, S.; Mély, Y.; Lenertz, M.; Wong, K.-L.; Platas-Iglesias, C.; Przybilla, F.; Charbonnière, L. J. Upconversion in a d–f [RuYb3] Supramolecular Assembly. *J. Am. Chem. Soc.* **2022**, *144* (29), 13356–13365. https://doi.org/10.1021/jacs.2c05037.
(21) Doffek, C.; Alzakhem, N.; Bischof, C.; Wahsner, J.; Güden-Silber, T.; Lügger, J.; Platas-Iglesias, C.; Seitz, M. Understanding the Quenching Effects of Aromatic C–H- and C–D-Oscillators in Near-IR Lanthanoid Luminescence. *J. Am. Chem. Soc.* **2012**, *134* (39), 16413–16423. https://doi.org/10.1021/ja307339f.
(22) Feng, Y.; Li, Z.; Li, Q.; Yuan, J.; Tu, L.; Ning, L.; Zhang, H. Internal OH − Induced Cascade Quenching of Upconversion Luminescence in NaYF 4 :Yb/Er Nanocrystals. *Light Sci. Appl.* **2021**, *10* (1), 105. https://doi.org/10.1038/s41377-021-00550-5.
(23) Pini, F.; Francés-Soriano, L.; Peruffo, N.; Barbon, A.; Hildebrandt, N.; Natile, M. M. Spatial and Temporal Resolution of Luminescence Quenching in Small Upconversion Nanocrystals. *ACS Appl. Mater. Interfaces* **2022**, *14* (9), 11883–11894. https://doi.org/10.1021/acsami.1c23498.
(24) Hyppänen, I.; Lahtinen, S.; Ääritalo, T.; Mäkelä, J.; Kankare, J.; Soukka, T. Photon Upconversion in a Molecular Lanthanide Complex in Anhydrous Solution at Room Temperature. *ACS Photonics* **2014**, *1* (5), 394–397. https://doi.org/10.1021/ph500047j.
(25) Golesorkhi, B.; Naseri, S.; Guénée, L.; Taarit, I.; Alves, F.; Nozary, H.; Piguet, C. Ligand-Sensitized Near-Infrared to Visible Linear Light Upconversion in a Discrete Molecular Erbium Complex. *J. Am. Chem. Soc.* **2021**, *143* (37), 15326–15334. https://doi.org/10.1021/jacs.1c06865.
(26) Taarit, I.; Alves, F.; Benchohra, A.; Guénée, L.; Golesorkhi, B.; Rosspeintner, A.; Fürstenberg, A.; Piguet, C. Seeking Brightness in Molecular Erbium-Based Light Upconversion. *J. Am. Chem. Soc.* **2023**. https://doi.org/10.1021/jacs.3c01331.
(27) Soro, L. K.; Knighton, R. C.; Avecilla, F.; Thor, W.; Przybilla, F.; Jeannin, O.; Esteban-Gomez, D.; Platas-Iglesias, C.; Charbonnière, L. J. Solution-State Cooperative Luminescence Upconversion in Molecular Ytterbium Dimers. *Adv. Opt. Mater.* **2023**, 2202307. https://doi.org/10.1002/adom.202202307.
(28) Knighton, R. C.; Soro, L. K.; Francés-Soriano, L.; Rodríguez-Rodríguez, A.; Pilet, G.; Lenertz, M.; Platas-Iglesias, C.; Hildebrandt, N.; Charbonnière, L. J. Cooperative Luminescence and Cooperative Sensitisation Upconversion of Lanthanide Complexes in Solution. *Angew. Chem. Int. Ed.* **2022**, *61* (4), e202113114. https://doi.org/10.1002/anie.202113114.
(29) Gálico, D. A.; Murugesu, M. Controlling the Energy-Transfer Processes in a Nanosized Molecular Upconverter to Tap into Luminescence Thermometry Application. *Angew. Chem. Int. Ed.* **2022**, *61* (29), e202204839. https://doi.org/10.1002/anie.202204839.
(30) Wen, S.; Zhou, J.; Zheng, K.; Bednarkiewicz, A.; Liu, X.; Jin, D. Advances in Highly Doped Upconversion Nanoparticles. *Nat. Commun.* **2018**, *9* (1), 2415. https://doi.org/10.1038/s41467-018-04813-5.
(31) Vera, V. T.; Mendez-Gonzalez, D.; Ramos-Ramos, D. J.; Igalla, A.; Laurenti, M.; Contreras-Caceres, R.; Lopez-Cabarcos, E.; Díaz, E.; Rubio-Retama, J.; Melle, S.; Calderón, O. G. The Effects of Dopant Concentration and Excitation Intensity on the Upconversion and Downconversion Emission Processes of β-NaYF4:Yb3+,Er3+ Nanoparticles. *J. Mater. Chem. C* **2021**, *9* (28), 8902–8911. https://doi.org/10.1039/D1TC01419F.
(32) Fu, H.; Hu, C.; Liu, J.; Zhang, Q.; Xu, J. Y.; Jiang, G. J.; Liu, M. An Overview of Boosting Lanthanide Upconversion Luminescence through Chemical Methods and Physical Strategies. *CrystEngComm.* **2022**, *24* (44), 7698–7717. https://doi.org/10.1039/D2CE01206E.
(33) Xiao, W.; Wu, D.; Zhang, L.; Zhang, X.; Hao, Z.; Pan, G.-H.; Zhao, H.; Zhang, L.; Zhang, J. Cooperative Upconversion Luminescence Properties of Yb3+ and Tb3+ Heavily Codoped Silicate Garnet Obtained

by Multiple Chemical Unit Cosubstitution. *J. Phys. Chem. C* **2017**, *121* (5), 2998–3006. https://doi.org/10.1021/acs.jpcc.6b11633.
(34) Prorok, K.; Olk, M.; Skowicki, M.; Kowalczyk, A.; Kotulska, A.; Lipiński, T.; Bednarkiewicz, A. Near-Infrared Excited Luminescence and in Vitro Imaging of HeLa Cells by Using Mn2+ Enhanced Tb3+ and Yb3+ Cooperative Upconversion in NaYF4 Nanocrystals. *Nanoscale Adv.* **2019**, *1* (9), 3463–3473. https://doi.org/10.1039/C9NA00336C.
(35) Sun, G.; Xie, Y.; Wang, Y.; Mandl, G. A.; Maurizio, S. L.; Zhang, H.; Ottenwaelder, X.; Capobianco, J. A.; Sun, L. Cooperative Sensitization Upconversion in Solution Dispersions of Co-Crystal Assemblies of Mononuclear Yb3+ and Eu3+ Complexes. *Angew. Chem. Int. Ed.* **2023**, *62* (24), e202304591. https://doi.org/10.1002/anie.202304591.
(36) Zare, D.; Suffren, Y.; Guénée, L.; Eliseeva, S. V.; Nozary, H.; Aboshyan-Sorgho, L.; Petoud, S.; Hauser, A.; Piguet, C. Smaller than a Nanoparticle with the Design of Discrete Polynuclear Molecular Complexes Displaying Near-Infrared to Visible Upconversion. *Dalton Trans.* **2015**, *44* (6), 2529–2540. https://doi.org/10.1039/C4DT02336F.
(37) Soro, L. K.; Charpentier, C.; Przybilla, F.; Mély, Y.; Nonat, A. M.; Charbonnière, L. J. Yb to Tb Cooperative Upconversion in Supramolecularly Assembled Complexes in a Solution. *Chemistry* **2021**, *3* (3), 1037–1046. https://doi.org/10.3390/chemistry3030074.
(38) Petit, S.; Baril-Robert, F.; Pilet, G.; Reber, C.; Luneau, D. Luminescence Spectroscopy of Europium(III) and Terbium(III) Penta-, Octa- and Nonanuclear Clusters with β-Diketonate Ligands. *Dalton Trans.* **2009**, No. 34, 6809–6815. https://doi.org/10.1039/B822883C.
(39) Dexter, D. L.; Schulman, J. H. Theory of Concentration Quenching in Inorganic Phosphors. *J. Chem. Phys.* **2004**, *22* (6), 1063–1070. https://doi.org/10.1063/1.1740265.
(40) Liu, J.; Fu, T.; Shi, C. Upconversion Model for Directly Determining the Microscopic Energy-Transfer Parameters for β-NaYF4:Er3+. *J. Phys. Chem. C* **2020**, *124* (46), 25509–25520. https://doi.org/10.1021/acs.jpcc.0c05305.
(41) Shaw, L. B.; Chang, R. S. F.; Djeu, N. Measurement of Up-Conversion Energy-Transfer Probabilities in Ho:Y3Al5O12 and Tm:Y3Al5O12. *Phys. Rev. B* **1994**, *50* (10), 6609–6619. https://doi.org/10.1103/PhysRevB.50.6609.
(42) Auzel, F. E. Materials and Devices Using Double-Pumped-Phosphors with Energy Transfer. *Proc. IEEE* **1973**, *61* (6), 758–786. https://doi.org/10.1109/PROC.1973.9155.
(43) Burshtein, A. I. Energy Transfer Kinetics in Disordered Systems. *J. Lumines.* **1985**, *34* (4), 167–188. https://doi.org/10.1016/0022-2313(85)90101-2.
(44) Burshteĭn, A. I. Concentration Quenching of Noncoherent Excitation in Solutions. *Sov. Phys. Usp.* **1984**, *27* (8), 579. https://doi.org/10.1070/PU1984v027n08ABEH004062.
(45) Inokuti, M.; Hirayama, F. Influence of Energy Transfer by the Exchange Mechanism on Donor Luminescence. *J. Chem. Phys.* **1965**, *43* (6), 1978–1989. https://doi.org/10.1063/1.1697063.
(46) Förster, Th. Zwischenmolekulare Energiewanderung und Fluoreszenz. *Ann. Phys. (Berl.)* **1948**, *437* (1–2), 55–75. https://doi.org/10.1002/andp.19484370105.
(47) Kushida, T. Energy Transfer and Cooperative Optical Transitions in Rare-Earth Doped Inorganic Materials. I. Transition Probability Calculation. *J. Phys. Soc. Jpn.* **1973**, *34* (5), 1318–1326. https://doi.org/10.1143/JPSJ.34.1318.
(48) Inokuti, M.; Hirayama, F. Influence of Energy Transfer by the Exchange Mechanism on Donor Luminescence. *J. Chem. Phys.* **2004**, *43* (6), 1978–1989. https://doi.org/10.1063/1.1697063.
(49) Dexter, D. L. A Theory of Sensitized Luminescence in Solids. *J. Chem. Phys.* **2004**, *21* (5), 836–850. https://doi.org/10.1063/1.1699044.
(50) Vergeer, P.; Vlugt, T. J. H.; Kox, M. H. F.; Hertog, M. I.; Eerden, J. P. J. M.; Meijerink, A. Quantum Cutting by Cooperative Energy Transfer in Yb x Y 1 − x P O 4 : Tb 3 +. *Phys. Rev. B* **2005**, *71* (1), 014119. https://doi.org/10.1103/PhysRevB.71.014119.
(51) Liu, J.; Fu, T.; Shi, C. Spatial Energy Transfer and Migration Model for Upconversion Dynamics in Core–Shell Nanostructures. *J. Phys. Chem. C* **2019**, *123* (14), 9506–9515. https://doi.org/10.1021/acs.jpcc.8b12300.

(52) Pilch-Wrobel, A.; Kotulska, A. M.; Lahtinen, S.; Soukka, T.; Bednarkiewicz, A. Engineering the Compositional Architecture of Core-Shell Upconverting Lanthanide-Doped Nanoparticles for Optimal Luminescent Donor in Resonance Energy Transfer: The Effects of Energy Migration and Storage. *Small* **2022**, *18* (18), 2200464. https://doi.org/10.1002/smll.202200464.
(53) Hossan, M. Y.; Hor, A.; Luu, Q.; Smith, S. J.; May, P. S.; Berry, M. T. Explaining the Nanoscale Effect in the Upconversion Dynamics of β-NaYF4:Yb3+, Er3+ Core and Core–Shell Nanocrystals. *J. Phys. Chem. C* **2017**, *121* (30), 16592–16606. https://doi.org/10.1021/acs.jpcc.7b04567.
(54) Krämer, K. W.; Biner, D.; Frei, G.; Güdel, H. U.; Hehlen, M. P.; Lüthi, S. R. Hexagonal Sodium Yttrium Fluoride Based Green and Blue Emitting Upconversion Phosphors. *Chem. Mater.* **2004**, *16* (7), 1244–1251. https://doi.org/10.1021/cm031124o.
(55) Chen, B.; Wang, F. Combating Concentration Quenching in Upconversion Nanoparticles. *Acc. Chem. Res.* **2020**, *53* (2), 358–367. https://doi.org/10.1021/acs.accounts.9b00453.